Available on the CERN CDS information server

CMS PAS HIN-16-018

CMS Physics Analysis Summary

Contact: cms-pag-conveners-heavyions@cern.ch

2017/02/07

Measurement of mixed higher order flow harmonics in PbPb collisions

The CMS Collaboration

Abstract

The mixed higher order flow harmonics and nonlinear response coefficients of charged particles are measured for the first time as a function of p_{T} and centrality in PbPb collisions at $\sqrt{s_{NN}} = 2.76$ TeV and 5.02 TeV with the CMS detector. The results are obtained using the scalar product method, and cover a p_{T} range from 0.3 GeV$/c$ to 8.0 GeV$/c$, pseudorapidity $|\eta| < 2.4$, and a centrality range of $0 - 60\%$. At 5.02 TeV, results for mixed harmonics are compared to the matching higher order flow harmonics from two-particle correlations, which measure v_n values with respect to the n-th order event plane. It is observed that the nonlinear response coefficients of the odd harmonics are larger than the even harmonics ones. The results are compared with hydrodynamic predictions with different shear viscosity to entropy density ratios and different initial conditions.

1 Introduction

Anisotropic flow plays a major role in probing the properties of the produced medium at the Relativistic Heavy Ion Collider (RHIC) at BNL and Large Hadron Collider (LHC) at CERN. The realization of higher order flow harmonics [1], flow fluctuations [2–5], the correlation between the magnitude and phase of different harmonics [6–9] and the $p_{\rm T}$ and η dependence of event plane angles [10, 11] has led to a broader and deeper understanding of the initial conditions and the properties of the produced hot and dense matter. The significant correlations [8] between the event plane angles of different order indicate that higher harmonics can be measured with respect to the direction of multiple lower order harmonics. Indeed, hydrodynamic predictions of the seventh flow harmonic with respect to the second and third order angles already exist [12].

The azimuthal anisotropy of particle production in an event can be characterized by a Fourier expansion of the distribution $P(\phi)$ in azimuthal angle ϕ [12],

$$P(\phi) = \frac{1}{2\pi} \sum_{n=-\infty}^{+\infty} V_n e^{-in\phi}, \tag{1}$$

where $V_n = v_n \exp(in\Psi_n)$ is the nth complex anisotropic flow coefficient. Both the magnitude, v_n, and phase, Ψ_n (also known as the event plane angle), of V_n fluctuate event to event [13]. In hydrodynamics, anisotropic flow results from the evolution of the medium in the presence of anisotropy in the initial density profile. The second and third harmonic coefficients, v_2 and v_3, are to a good approximation linearly proportional to the initial state anisotropies, ϵ_2 and ϵ_3 [1, 6]. In contrast, V_4 and higher harmonics can arise from initial state anisotropies in the same order harmonic (linear response) or can be induced by lower order harmonics (nonlinear response) [12, 14, 15]. To a good approximation, the nonlinear contribution to these higher order harmonics can be written in terms of the two largest anisotropic flow coefficients V_2 and V_3 [12, 14],

$$\begin{aligned}
V_4 &= V_{4L} + \chi_{422}(V_2)^2 \\
V_5 &= V_{5L} + \chi_{523} V_2 V_3 \\
V_6 &= V_{6L} + \chi_{6222}(V_2)^3 + \chi_{633}(V_3)^2 \\
V_7 &= V_{7L} + \chi_{7223}(V_2)^2 V_3,
\end{aligned} \tag{2}$$

where V_{nL} denotes the part of V_n due to linear response, and the χ are the nonlinear response coefficients.

The properties of the produced medium in heavy ion collisions is poorly understood so far for the stage close to the freeze-out temperature. Recent studies show that the nonlinear response coefficients probe the properties of the system at freeze-out and are weekly sensitive to the initial density fluctuations [12, 14]. Most previous flow measurements focused on measuring V_n, i.e. v_n with respect to Ψ_n which can not separate the linear and nonlinear parts of Eq. (2). Direct measurements of the mixed higher order flow harmonics, $v_4\{\Psi_2\}$ and $v_6\{\Psi_2\}$, already exist from both RHIC and LHC energies [16, 17], but were using the event plane method which was recently criticized for yielding an ambiguous measurement, neither the mean value $\langle v_n \rangle$ nor the root-mean-square value $\langle v_n^2 \rangle^{1/2}$ [18]. This ambiguity can be removed by using the scalar product method, which always measures the root-mean-square of v_n distribution. The difference between the two methods is typically a few percent for v_2, $\sim 10\%$ for v_3 and much larger for mixed harmonics [18]. To study the nonlinear part of Eq. (2), this paper presents the mixed higher order flow harmonics, v_4 with respect to Ψ_2 ($v_4\{\Psi_{22}\}$), v_5 with respect to Ψ_2 and Ψ_3 ($v_5\{\Psi_{23}\}$), v_6 with respect to Ψ_2 ($v_6\{\Psi_{222}\}$), v_6 with respect to Ψ_3 ($v_6\{\Psi_{33}\}$), v_7 with respect to Ψ_2 and Ψ_3 ($v_7\{\Psi_{223}\}$), and the nonlinear response coefficients χ_{422}, χ_{523}, χ_{6222}, χ_{633} and χ_{7223} using the scalar product method. These variables are measured in PbPb collisions at $\sqrt{s_{NN}}$ = 2.76 TeV and 5.02 TeV as a function of p_{T} and collision centrality in the pseudorapidity region of $|\eta| < 2.4$, where $\eta = -\ln[\tan(\theta/2)]$ and θ is the polar angle relative to the counterclockwise beam direction. The results in this paper represent the first measurements of these variables, which will help constrain the theoretical description of the medium close the freeze-out temperature.

To compare the mixed flow harmonics with the overall flow coefficients, the higher order flow harmonics with respect to the event plane of the same order measured from two-particle correlations constructed using the standard CMS approach [19–22] are also presented.

2 CMS Detector

The CMS detector comprises a number of subsystems. A detailed description of the CMS detector can be found in Ref. [23]. The results in this paper are mainly based on the silicon tracker and hadron forward calorimeters. The silicon tracker is located in the 3.8 T field of the superconducting solenoid and consists of 1440 silicon pixel and 15 148 silicon strip detector modules. It measures charged particles within the pseudorapidity range $|\eta| < 2.5$, and provides an impact parameter resolution of $\approx 15\,\mu$m and a p_{T} resolution better than 1.5% up to $p_{\mathrm{T}} = 100$ GeV/c. Iron hadron-forward (HF) calorimeters, with quartz fibers read out by photomultipliers, cover a pseudorapidity range of 2.9< $|\eta|$ <5.2 on either side of the interaction region. These calorimeters are azimuthally subdivided into 20° modular wedges and further segmented to form 0.175×0.175 ($\Delta\eta \times \Delta\phi$) "towers", where the angle ϕ is in radians The Monte Carlo (MC) simulation of the CMS detector response is based on GEANT4 [24].

3 Event and track selections

3.1 Event selections

This analysis is performed using about 100 million minimum-bias events at $\sqrt{s_{NN}}$ = 5.02 TeV and about 30 million events at $\sqrt{s_{NN}}$ = 2.76 TeV. The minimum-bias trigger used in this analysis is required to be in coincidence with colliding bunches. This is insured by requiring coincidence signals in the Beam Pickup Timing for the eXperiment detector and at least a HF tower on each side with an energy signal. This requirement allows to largely suppress events due to noise, cosmic rays and beam backgrounds. The collected events are cleaned for detector noise with the use of a hadronic calorimeter (HCAL, $2.5 < |\eta| < 5.2$) noise cleaning filter, and electromagnetic calorimeter (ECAL, $|\eta| < 2.4$) spike removal.

In the offline analysis, events are required to have at least one reconstructed primary vertex. The primary vertex is formed by two or more associated tracks and is required to have a distance of less than 15 cm along the beam axis from the center of the nominal interaction region and less than 0.15 cm from the beam position in the transverse plane. An additional selection of hadronic collisions is applied by requiring a coincidence of at least one of the HF calorimeter towers, with more than 3 GeV of total energy, from the HF detectors on both sides of the interaction point. Events are classified using a variable called centrality, which is related to the degree of geometric overlap within the two colliding nuclei. Events with complete (no) overlap are denoted as centrality 0% (100%), where the number is the fraction of the total hadronic inelastic cross section. The centrality is measured offline via the sum of the HF energies in each event. Very central events (centrality approaching 0%) are characterized by a large energy deposit in the HF calorimeters. The minimum-bias trigger and event selections are fully efficient for the centrality range 0-90%.

3.2 Track selections

In this analysis, the *high-purity* tracks (as defined in Ref. [25]) are used to select primary-track candidates and perform correlation measurements. Additional requirements are also applied to enhance the purity of primary tracks. The significance of the separation along the beam axis (z) between the track and the primary vertex, $d_z/\sigma(d_z)$, and the significance of the impact parameter relative to the primary vertex transverse to the beam, $d_{\mathrm{T}}/\sigma(d_{\mathrm{T}})$, must be less than 3. The relative uncertainty of the transverse-momentum measurement, $\sigma(p_{\mathrm{T}})/p_{\mathrm{T}}$, must be less than 10%. The analysis is done using tracks within $|\eta| < 2.4$ and a p_{T} range from 0.3 GeV/c to 8.0 GeV/c. The tracking efficiency and the rate of misreconstructed tracks are evaluated as a function of centrality, vertex location in the z direction, as well as track p_{T} and η by propagating simulated PbPb events, generated using HYDJET [26], through the detector using GEANT4 [24]. Primary track reconstruction has a combined geometric acceptance and efficiency exceeding 70% for $p_{\mathrm{T}} \approx 1.0$ GeV/c and $|\eta| < 1.0$. The efficiency is not strongly dependent on centrality and the rate of misreconstructed tracks is smaller than 8% for the most central events. The measured flow and nonlinear response coefficients are corrected for tracking efficiency and misreconstructed tracks.

4 Analysis technique

The analysis technique in this paper follows the method described in [12, 14]. The notation $V_n = v_n \exp(in\Psi_n) = \langle e^{in\phi} \rangle$ in Eq. (1) will be replaced with the measured flow vector $Q_n = (|Q_n|\cos(n\Psi_n), |Q_n|\sin(n\Psi_n))$. Equivalently, it is a complex variable $Q_n = |Q_n|e^{in\Psi_n} = \langle e^{in\phi} \rangle$ with real and imaginary parts defined as

$$Re(Q_n) = |Q_n|\cos(n\Psi_n) = \frac{1.0}{\sum w_j}\sum_j^M w_j \cos\left(n\phi_j\right) - \left\langle \frac{1.0}{\sum w_j}\sum_j^M w_j \cos\left(n\phi_j\right) \right\rangle_{evts} \tag{3}$$

$$Im(Q_n) = |Q_n|\sin(n\Psi_n) = \frac{1.0}{\sum w_j}\sum_j^M w_j \sin\left(n\phi_j\right) - \left\langle \frac{1.0}{\sum w_j}\sum_j^M w_j \sin\left(n\phi_j\right) \right\rangle_{evts} \tag{4}$$

where weight w_j is the transverse energy in each HF tower j, M is the number of HF tower used for calculating the Q vector, $\langle \ldots \rangle_{evts}$ denotes average over all the events in a centrality range. Only towers with transverse energy larger than 0.005 GeV were considered. Subtraction of the event-averaged quantity removes biases due to detector effects. For Q vectors calculated using a sum over tracks, the tracking inefficiency and the effect of misreconstructed tracks are corrected for by using weight $w_j = (1-F)/E$, where E is the absolute tracking inefficiency and F is the rate of misreconstructed tracks.

4.1 Mixed higher order flow harmonics

With the scalar product method, the differential mixed higher order harmonics in each p_{T} bin can be expressed as [12],

$$v_4\{\Psi_{22}\} = \frac{\mathrm{Re}\langle e^{4i\phi} Q_{2B}^* Q_{2B}^* \rangle}{\sqrt{\mathrm{Re}\langle Q_{2A} Q_{2A} Q_{2B}^* Q_{2B}^* \rangle}} \tag{5}$$

$$v_5\{\Psi_{23}\} = \frac{\mathrm{Re}\langle e^{5i\phi} Q_{2B}^* Q_{3B}^* \rangle}{\sqrt{\mathrm{Re}\langle Q_{2A} Q_{3A} Q_{2B}^* Q_{3B}^* \rangle}} \tag{6}$$

$$v_6\{\Psi_{222}\} = \frac{\mathrm{Re}\langle e^{6i\phi} Q_{2B}^* Q_{2B}^* Q_{2B}^* \rangle}{\sqrt{\mathrm{Re}\langle Q_{2A} Q_{2A} Q_{2A} Q_{2B}^* Q_{2B}^* Q_{2B}^* \rangle}} \tag{7}$$

$$v_6\{\Psi_{33}\} = \frac{\mathrm{Re}\langle e^{6i\phi} Q_{3B}^* Q_{3B}^* \rangle}{\sqrt{\mathrm{Re}\langle Q_{3A} Q_{3A} Q_{3B}^* Q_{3B}^* \rangle}} \tag{8}$$

$$v_7\{\Psi_{223}\} = \frac{\mathrm{Re}\langle e^{7i\phi} Q_{2B}^* Q_{2B}^* Q_{3B}^* \rangle}{\sqrt{\mathrm{Re}\langle Q_{2A} Q_{2A} Q_{3A} Q_{2B}^* Q_{2B}^* Q_{3B}^* \rangle}} \tag{9}$$

where Q_{nA} and Q_{nB} are two subevents from two different parts of the detector, specifically the positive and negative side of HF, ϕ is the azimuthal angle of the charged particle. The average in the numerator is an average over particles in a considered p_T bin for all the events in a centrality range. The average in the denominator is an average over events in a centrality range. If the η of a charged particle is positive (negative) then in the above formulas, Q_{nB} is using the negative (positive) side of HF and Q_{nA} is from the positive (negative) side of HF. This ensures that the minimum η gap between the charged particle and Q vector in the numerator is at least 3 units of pseudorapidity. The mixed higher order harmonics as a function of centrality are obtained by averaging the differential v_n over p_T with the charged particle spectra yield in each p_T bin as weights.

4.2 Nonlinear response coefficients

Similar to the mixed higher order flow harmonics, the differential nonlinear response coefficients in each p_T bin can be expressed as [12],

$$\chi_{422} = \frac{\mathrm{Re}\langle e^{4i\phi} Q_{2B}^* Q_{2B}^* \rangle}{\mathrm{Re}\langle Q_{2Atrk} Q_{2Atrk} Q_{2B}^* Q_{2B}^* \rangle} \tag{10}$$

$$\chi_{523} = \frac{\mathrm{Re}\langle e^{5i\phi} Q_{2B}^* Q_{3B}^* \rangle}{\mathrm{Re}\langle Q_{2Atrk} Q_{3Atrk} Q_{2B}^* Q_{3B}^* \rangle} \tag{11}$$

$$\chi_{6222} = \frac{\mathrm{Re}\langle e^{6i\phi} Q_{2B}^* Q_{2B}^* Q_{2B}^* \rangle}{\mathrm{Re}\langle Q_{2Atrk} Q_{2Atrk} Q_{2Atrk} Q_{2B}^* Q_{2B}^* Q_{2B}^* \rangle} \tag{12}$$

$$\chi_{633} = \frac{\mathrm{Re}\langle e^{6i\phi} Q_{3B}^* Q_{3B}^* \rangle}{\mathrm{Re}\langle Q_{3Atrk} Q_{3Atrk} Q_{3B}^* Q_{3B}^* \rangle} \tag{13}$$

$$\chi_{7223} = \frac{\mathrm{Re}\langle e^{7i\phi} Q_{2B}^* Q_{2B}^* Q_{3B}^* \rangle}{\mathrm{Re}\langle Q_{2Atrk} Q_{2Atrk} Q_{3Atrk} Q_{2B}^* Q_{2B}^* Q_{3B}^* \rangle} \tag{14}$$

where Q_{nAtrk} is the Q vector obtained from charged particle tracks in the same η range as particles used in $e^{ni\phi}$ in the numerator. The nonlinear response coefficients as a function of centrality are obtained by averaging the differential χ over p_T with charged particle spectra yield in each p_T bin as weights.

4.3 Flow harmonics from two-particle correlations

The construction of the two-dimensional (2D) two-particle correlation function follows its standard definition within the CMS experiment [22, 27]. Any charged particle from the $|\eta| < 2.4$ range is used as a 'trigger' particle. As there can be more than one trigger particle in an event from a given p_{T} interval, the corresponding total number of trigger particles is denoted by N_{trig}. In order to construct the 2D two-particle correlation function, in each event, every trigger particle is paired with all of the remaining charged particles from the $|\eta| < 2.4$ range which belong to a required p_{T} interval. Then, the signal distribution, $S(\Delta\eta, \Delta\phi)$, is defined as the per-trigger-particle yield of pairs within the same event,

$$S(\Delta\eta, \Delta\phi) = \frac{1}{N_{trig}} \frac{d^2 N^{same}}{d\Delta\eta d\Delta\phi} \tag{15}$$

In Eq. (15), N^{same} denotes the per-trigger-particle pairs yield within a given $(\Delta\eta, \Delta\phi)$ bin where $\Delta\eta$ and $\Delta\phi$ are corresponding differences in pseudorapidity and azimuthal angle between the two charged particles which are forming a pair. The background distribution, $B(\Delta\eta, \Delta\phi)$, is constructed using the technique of mixing events with similar multiplicity and vertex position. The mixing technique ensure that particles which form a given pair are not physically correlated. Technically, the mixing of events means that the trigger particles from one event are combined (mixed) with all of the associated particles from a different event. In order to reduce contribution to the statistical uncertainty from the background distribution, associated particles from 10 randomly chosen events are used. The background distribution is then defined as

$$B(\Delta\eta, \Delta\phi) = \frac{1}{N_{trig}} \frac{d^2 N^{mix}}{d\Delta\eta d\Delta\phi}, \tag{16}$$

where N^{mix} denotes the number of mixed-event pairs in a given $(\Delta\eta, \Delta\phi)$ bin. Due to the fact that pairs are formed from uncorrelated particles, the background should represent a distribution of independent particle emission, but at the same time it takes into account effects of the finite detector acceptance. Each particle is weighted by a correction factor that account for the tracking inefficiency and the rate of misreconstructed tracks as described in Refs. [22, 27].

The 2D two-particle differential correlation function is then defined as the normalized ratio of the *signal* to the *background* distribution

$$\frac{1}{N_{trig}} \frac{d^2 N^{pair}}{d\Delta\eta d\Delta\phi} = B(0,0) \frac{S(\Delta\eta, \Delta\phi)}{B(\Delta\eta, \Delta\phi)} \tag{17}$$

The normalization factor, B(0, 0), as the value of the background distribution at $\Delta\eta = 0$ and $\Delta\phi = 0$ bin, is used to account for the finite pair-acceptance effect.

In order to obtain the single-particle azimuthal anisotropy harmonics, v_n, and to provide enough statistics, the $2 < |\Delta\eta| < 4$ region of the 2D two-particle correlation function given by Eq. (17) is first projected onto $\Delta\phi$ axis. The restriction over the $|\Delta\eta| > 2$ region is done in order to avoid the short-range correlations from jets and resonance decays. Such a projection can be then Fourier decomposed and the differential in p_{T} Fourier $V_{n\Delta}$ coefficients are obtained. Finally, the differential single-particle Fourier coefficients $v_n(p_{\mathrm{T}})$ as a function of p_{T} are extracted.

4.4 Systematic uncertainties

Six sources of systematic uncertainties are considered. The systematic uncertainty on the vertex position cuts is estimated by comparing the results with events from different vertex position ranges. The track quality cut systematic uncertainty is obtained by varying the track selections for $d_z/\sigma(d_z)$ and $d_T/\sigma(d_T)$ from 2 to 5. The tracking efficiency uncertainty is studied with different tracking efficiencies from different tracking software. Although the trigger and event selections are fully efficient in the 0-60% centrality range, the centrality bins will have a small shift because of the uncertainty of event selection efficiency. The difference between results before and after the small shift is taken as the systematic uncertainty from the trigger and event selections. When the same set of HF towers are used for different Q vectors in the equations of mixed harmonics and nonlinear response coefficients, the product of these Q vectors contains self-correlations. An algorithm for removing the self-correlations is designed and the difference before and after correcting this effect is taken as the systematic uncertainty. A summary of different sources of systematic uncertainties for the mixed higher order flow harmonics is given in Table 1.

Table 1: Summary of different sources of systematic uncertainties for each mixed higher order flow harmonic.

Source	$v_4\{\Psi_{23}\}$	$v_5\{\Psi_{23}\}$	$v_6\{\Psi_{222}\}$	$v_6\{\Psi_{33}\}$	$v_7\{\Psi_{223}\}$
Vertex Position	3%	5%	6%	6%	7%
Track Quality Cuts	3%	3%	3%	3%	3%
Tracking Efficiency	3%	3%	3%	3%	3%
Event Selections	1%	1%	1%	1%	1%
Self-Correlations	3%	3%	3%	3%	3%

The systematic uncertainties for the nonlinear response coefficients, χ_{422}, χ_{523}, χ_{6222}, χ_{633} and χ_{7223} are the same as the corresponding mixed higher order flow harmonics, $v_4\{\Psi_{22}\}$, $v_5\{\Psi_{23}\}$, $v_6\{\Psi_{222}\}$, $v_6\{\Psi_{33}\}$ and $v_7\{\Psi_{223}\}$ for the 5 systematic studies in the table. The uncertainties are found not to depend on p_T or centrality. The effect of changing the eta gap between the region used for charged particles and that used for the Q vector in the HF region is studied. By varying the minimum η gap from 3–3.5 to 3.5–4.0 and then to 4.0–5.0 (compared to the default of 3.0–5.0), the absolute systematic uncertainties are estimated to be in the range from 0.0002 to 0.0003 for mixed harmonics and from 0.02 to 0.4 for nonlinear response coefficients. The systematic uncertainties of the v_n harmonics extracted from two-particle correlations are obtained by varying the vertex position from $|v_z| < 15$ cm to $|v_z| < 3$, and the track quality selections, $d_z/\sigma(d_z)$ and $d_T/\sigma(d_T)$, from 2 to 5. The total systematic uncertainties in the two-particle v_n values are 4% for $n = 4$ and $n = 5$, 5% for $n = 6$, and 9% for $n = 7$.

5 Results

Figure 1 shows the mixed higher order flow harmonics, $v_4\{\Psi_{22}\}$, $v_5\{\Psi_{23}\}$, $v_6\{\Psi_{222}\}$, $v_6\{\Psi_{33}\}$ and $v_7\{\Psi_{223}\}$ from the scalar product method at 2.76 and 5.02 TeV as a function of p_T with $|\eta| < 2.4$ in the 0-20% (top row) and 20-60% (bottom row) centrality ranges. It is observed that the shape of the mixed higher order flow harmonics as a function of p_T are qualitatively similar to the published flow harmonics [17], first increasing at low p_T, reaching a maximum at about 3-4 GeV/c then decreasing at higher p_T. The values of $v_4\{\Psi_{22}\}$ and $v_5\{\Psi_{23}\}$ are larger than $v_6\{\Psi_{222}\}$, $v_6\{\Psi_{33}\}$ and $v_7\{\Psi_{223}\}$ in the same centrality range.

The flow harmonics from two-particle correlations, denoted as, $v_4\{|\Delta\eta| > 2\}$, $v_5\{|\Delta\eta| > 2\}$, $v_6\{|\Delta\eta| > 2\}$ and $v_7\{|\Delta\eta| > 2\}$ are studied as a function of p_T and centrality at 5.02 TeV. These results are the total flow on the left hand side of Eq. (2). The mixed harmonics in Fig. 1 are the nonlinear part, the second term on the right hand side of Eq. (2). Comparisons of mixed higher order flow harmonics and flow from two-particle correlations at 5.02 TeV are presented

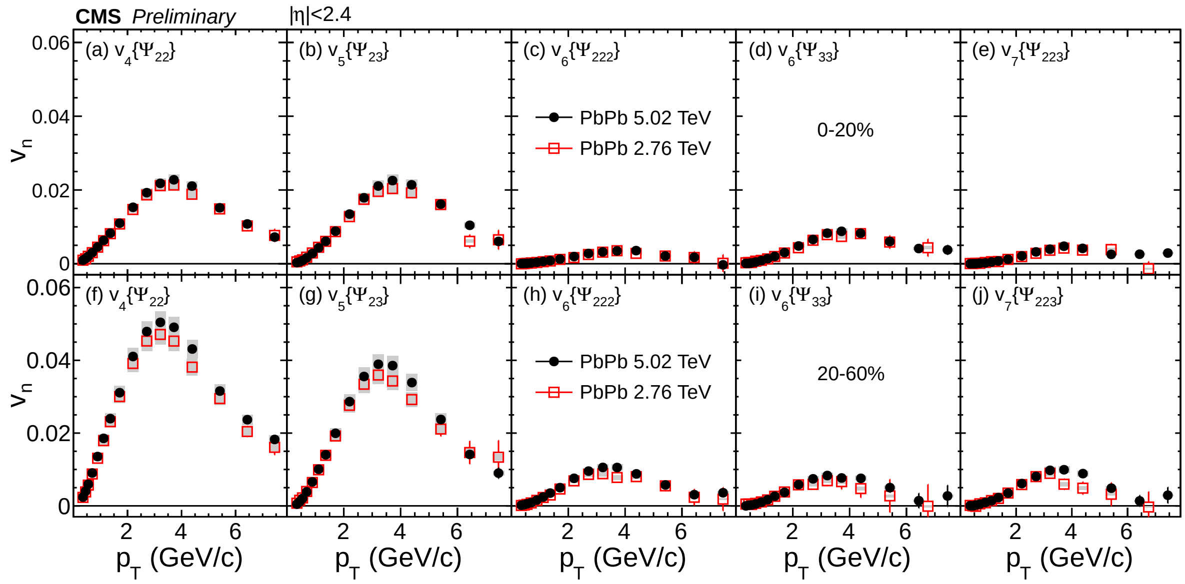

Figure 1: The mixed higher order flow harmonics, $v_4\{\Psi_{22}\}$, $v_5\{\Psi_{23}\}$, $v_6\{\Psi_{222}\}$, $v_6\{\Psi_{33}\}$ and $v_7\{\Psi_{223}\}$ from the scalar product method at 2.76 and 5.02 TeV as a function of p_T with $|\eta| < 2.4$ in the 0-20% (top row) and 20-60% (bottom row) centrality ranges. Statistical (error bars) and systematic (shaded boxes) uncertainties are shown.

in Fig. 2 as a function p_T with $|\eta| < 2.4$ in the 0-20% (top row) and 20-60% (bottom row) centrality ranges. The contribution of the nonlinear part for v_5 and v_7 are larger than those for the other harmonics in the centrality range 20-60%.

The nonlinear response coefficients, χ_{422}, χ_{523}, χ_{6222}, χ_{633} and χ_{7223} are presented in Fig. 3 as a function of p_T with $|\eta| < 2.4$ in the 0-20% (top row) and 20-60% (bottom row) centrality ranges at 2.76 and 5.02 TeV. It is clearly observed that the nonlinear response coefficients of the odd harmonics , χ_{523} and χ_{7223}, are larger than those for the even harmonics.

Figure 4 shows the mixed higher order flow harmonics, $v_4\{\Psi_{22}\}$, $v_5\{\Psi_{23}\}$, $v_6\{\Psi_{222}\}$, $v_6\{\Psi_{33}\}$ and $v_7\{\Psi_{223}\}$ from the scalar product method at 2.76 and 5.02 TeV as a function of centrality with $|\eta| < 2.4$ in the $0.3 < p_T < 3.0$ GeV/c range. The hydrodynamic predictions with a deformed symmetric Gaussian density profile as the initial condition for $v_5\{\Psi_{23}\}$ and $v_7\{\Psi_{223}\}$ [12] are compared with data. The model qualitatively describes the shape of $v_5\{\Psi_{23}\}$ as a function centrality, but shows large discrepancies for $v_7\{\Psi_{223}\}$ in mid-central and peripheral collisions.

The nonlinear response coefficients, χ_{422}, χ_{523}, χ_{6222}, χ_{633} and χ_{7223} are presented in Figs. 5 and 6 as a function of centrality with $|\eta| < 2.4$ in the $0.3 < p_T < 3.0$ GeV/c range. In Fig. 5, the results are compared with predictions from AMPT and hydrodynamics with a deformed symmetric Gaussian density profile as the initial condition using $\eta/s = 0.08$ in Ref. [12], and from iEBE-VISHNU hydrodynamics with Glauber and KLN initial conditions using the same η/s [14]. Predictions from AMPT are favored by the measurement. In Fig. 6, the same results are compared with predictions from AMPT in Ref. [12] and from iEBE-VISHNU hydrodynamics with KLN initial condition using $\eta/s = 0$, 0.08 and 0.2 [14]. The large difference between hydrodynamic predictions with different viscosities indicates that our results can provide constraints on the value of viscosity at freeze-out [12, 14]. However, based only on these comparisons, it is not unambiguously clear which viscosity and initial conditions are the best choices.

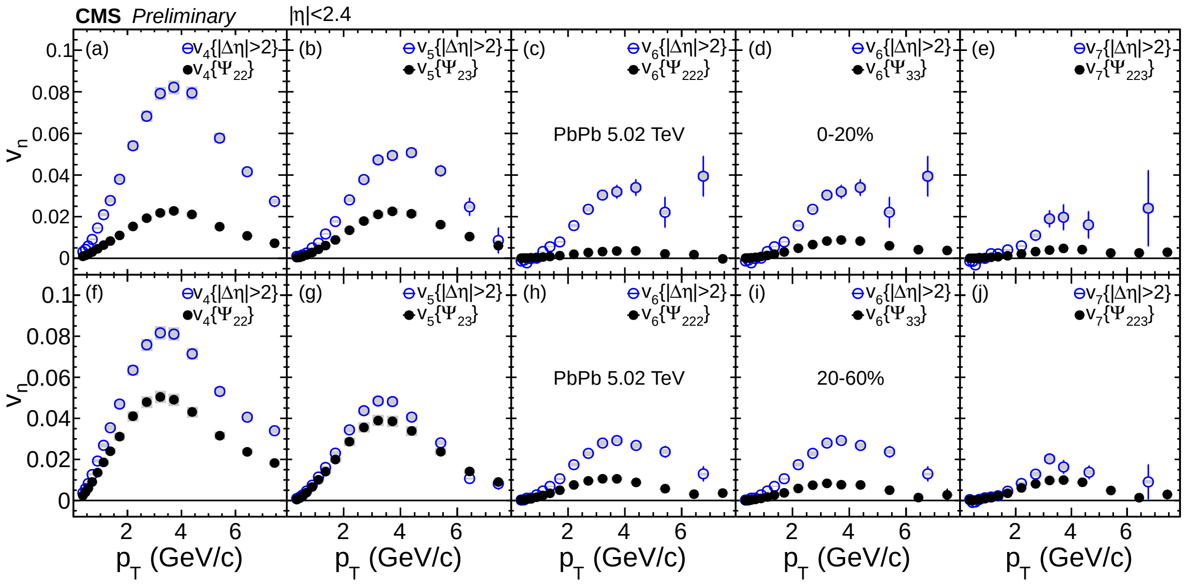

Figure 2: Comparison of mixed higher order flow harmonics and flow from two-particle correlations at 5.02 TeV as a function p_T with $|\eta| < 2.4$ in the 0-20% (top row) and 20-60% (bottom row) centrality ranges. Statistical (error bars) and systematic (shaded boxes) uncertainties are shown.

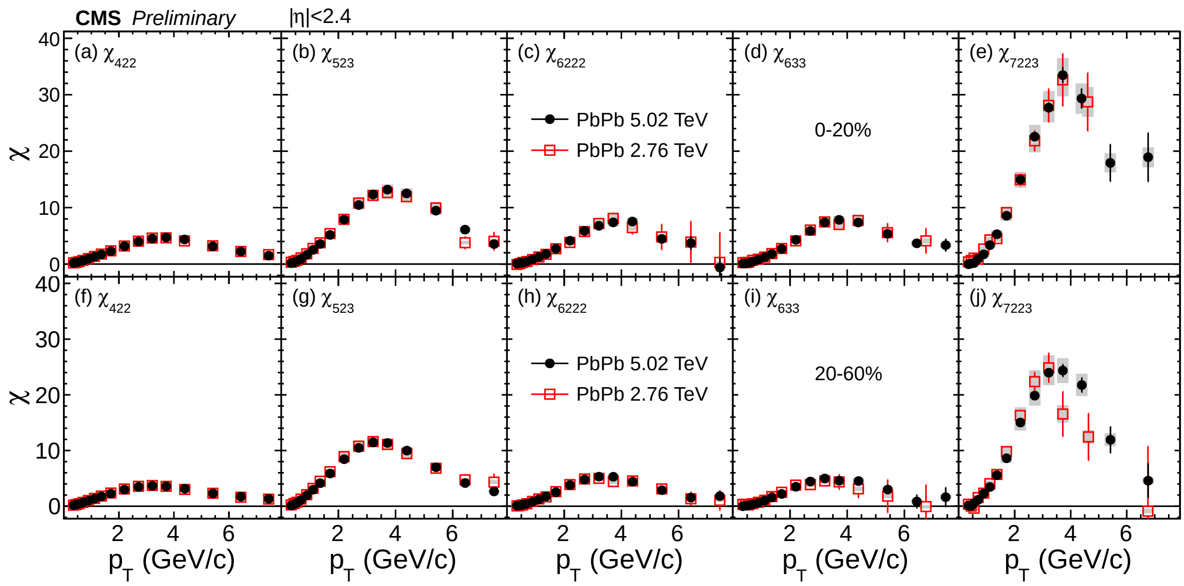

Figure 3: The nonlinear response coefficients, χ_{422}, χ_{523}, χ_{6222}, χ_{633} and χ_{7223} from the scalar product method at 2.76 and 5.02 TeV as a function of p_T with $|\eta| < 2.4$ in the 0-20% (top row) and 20-60% (bottom row) centrality ranges. Statistical (error bars) and systematic (shaded boxes) uncertainties are shown.

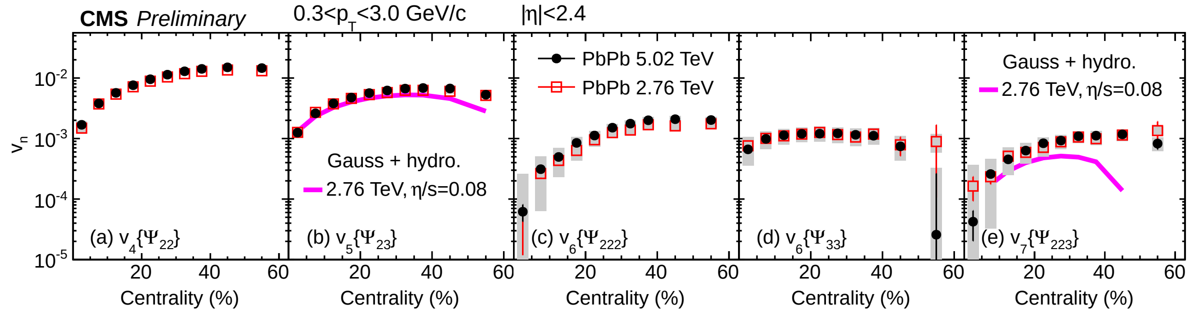

Figure 4: The mixed higher order flow harmonics, $v_4\{\Psi_{22}\}$, $v_5\{\Psi_{23}\}$, $v_6\{\Psi_{222}\}$, $v_6\{\Psi_{33}\}$ and $v_7\{\Psi_{223}\}$ from the scalar product method at 2.76 and 5.02 TeV as a function of centrality with $|\eta| < 2.4$ in the $0.3 < p_{\mathrm{T}} < 3.0$ GeV/c range. Statistical (error bars) and systematic (shaded boxes) uncertainties are shown. The hydrodynamic predictions [12] with η/s =0.08 (magenta lines) are compared with data.

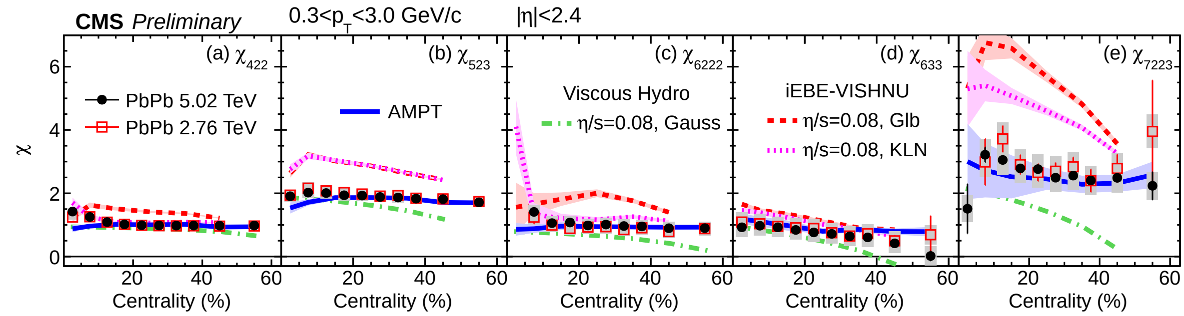

Figure 5: The nonlinear response coefficients, χ_{422}, χ_{523}, χ_{6222}, χ_{633} and χ_{7223} from the scalar product method at 2.76 and 5.02 TeV as a function of centrality with $|\eta| < 2.4$ in the $0.3 < p_{\mathrm{T}} < 3.0$ GeV/c range. Statistical (error bars) and systematic (shaded boxes) uncertainties are shown. The results are compared with predictions from AMPT and hydrodynamics with a deformed symmetric Gaussian density profile as the initial condition using $\eta/s = 0.08$ in Ref. [12], and from iEBE-VISHNU hydrodynamics with Glauber and KLN initial conditions using the same η/s [14].

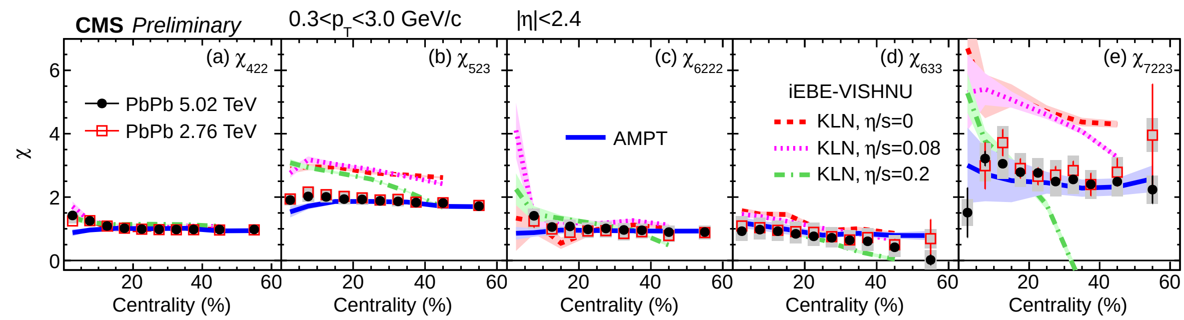

Figure 6: The nonlinear response coefficients, χ_{422}, χ_{523}, χ_{6222}, χ_{633} and χ_{7223} from the scalar product method at 2.76 and 5.02 TeV as a function of centrality with $|\eta| < 2.4$ in the $0.3 < p_{\mathrm{T}} < 3.0$ GeV/c range. Statistical (error bars) and systematic (shaded boxes) uncertainties are shown. The results are compared with predictions from AMPT in Ref. [12] and from iEBE-VISHNU hydrodynamics with KLN initial condition using $\eta/s = 0$, 0.08 and 0.2 [14].

6 Summary

The mixed higher order flow harmonics and nonlinear response coefficients of charged particles has been studied for the first time as a function of p_{T} and centrality in PbPb collisions at $\sqrt{s_{NN}}$ = 2.76 TeV and 5.02 TeV using the CMS detector. The measurements are done with the scalar product method, covering a p_{T} range from 0.3 GeV/c to 8.0 GeV/c, $|\eta| < 2.4$ and centrality range of 0-60%. Additionally, as a comparison, v_n harmonics $(n = 4, ..., 7)$ are measured with the two-particle correlation method over $0.3 < p_{\mathrm{T}} < 8.0$ GeV/c and $|\eta| <2.4$ and within the same centrality range. The shape of the mixed higher order flow harmonics, $v_4\{\Psi_{22}\}$, $v_5\{\Psi_{23}\}$, $v_6\{\Psi_{222}\}$, $v_6\{\Psi_{33}\}$ and $v_7\{\Psi_{223}\}$, and nonlinear response coefficients, χ_{422}, χ_{523}, χ_{6222}, χ_{633} and χ_{7223} as a function p_{T} are similar, first increases at low p_{T}, reach maximum at about 3-4 GeV/c then decreases at higher p_{T}. The contribution of nonlinear part for v_5 and v_7 are larger than other harmonics in the centrality range 20-60%. It is clearly observed that the nonlinear response coefficients of the odd harmonics, χ_{523} and χ_{7223}, are larger than the even harmonics. The data are compared with AMPT and hydrodynamic predictions with different shear viscosity to entropy density ratios and initial condition models. The predictions from AMPT are favored by the measurement. These results will provide constraints on the theoretical description of the medium close to the freeze-out temperature, which is poorly understood so far.

References

[1] B. Alver and G. Roland, "Collision geometry fluctuations and triangular flow in heavy-ion collisions", *Phys. Rev. C* **81** (2010) 054905, doi:10.1103/PhysRevC.82.039903,10.1103/PhysRevC.81.054905, arXiv:1003.0194. [Erratum: Phys. Rev.C82,039903(2010)].

[2] B. Alver et al., "Importance of correlations and fluctuations on the initial source eccentricity in high-energy nucleus-nucleus collisions", *Phys. Rev. C* **77** (2008) 014906, doi:10.1103/PhysRevC.77.014906, arXiv:0711.3724.

[3] STAR Collaboration, "Elliptic flow fluctuations in Au + Au collisions at s(NN)**(1/2) = 200-GeV", *J. Phys. G* **35** (2008) 104102, doi:10.1088/0954-3899/35/10/104102, arXiv:0808.0356.

[4] PHOBOS Collaboration, "Non-flow correlations and elliptic flow fluctuations in gold-gold collisions at $\sqrt{s_{NN}} = 200$ GeV", *Phys. Rev. C* **81** (2010) 034915, doi:10.1103/PhysRevC.81.034915, arXiv:1002.0534.

[5] J.-Y. Ollitrault, A. M. Poskanzer, and S. A. Voloshin, "Effect of flow fluctuations and nonflow on elliptic flow methods", *Phys. Rev. C* **80** (2009) 014904, doi:10.1103/PhysRevC.80.014904, arXiv:0904.2315.

[6] Z. Qiu and U. W. Heinz, "Event-by-event shape and flow fluctuations of relativistic heavy-ion collision fireballs", *Phys. Rev. C* **84** (2011) 024911, doi:10.1103/PhysRevC.84.024911, arXiv:1104.0650.

[7] PHENIX Collaboration, "Measurements of Higher-Order Flow Harmonics in Au+Au Collisions at $\sqrt{s_{NN}} = 200$ GeV", *Phys. Rev. Lett.* **107** (2011) 252301, doi:10.1103/PhysRevLett.107.252301, arXiv:1105.3928.

[8] ATLAS Collaboration, "Measurement of event-plane correlations in $\sqrt{s_{NN}} = 2.76$ TeV lead-lead collisions with the ATLAS detector", *Phys. Rev. C* **90** (2014), no. 2, 024905, doi:10.1103/PhysRevC.90.024905, arXiv:1403.0489.

[9] ATLAS Collaboration, "Measurement of the correlation between flow harmonics of different order in lead-lead collisions at $\sqrt{s_{NN}}$=2.76 TeV with the ATLAS detector", *Phys. Rev. C* **92** (2015), no. 3, 034903, doi:10.1103/PhysRevC.92.034903, arXiv:1504.01289.

[10] U. Heinz, Z. Qiu, and C. Shen, "Fluctuating flow angles and anisotropic flow measurements", *Phys. Rev. C* **87** (2013), no. 3, 034913, doi:10.1103/PhysRevC.87.034913, arXiv:1302.3535.

[11] CMS Collaboration, "Evidence for transverse momentum and pseudorapidity dependent event plane fluctuations in PbPb and pPb collisions", *Phys. Rev. C* **92** (2015), no. 3, 034911, doi:10.1103/PhysRevC.92.034911, arXiv:1503.01692.

[12] L. Yan and J.-Y. Ollitrault, "v_4, v_5, v_6, v_7: nonlinear hydrodynamic response versus LHC data", *Phys. Lett. B* **744** (2015) 82–87, doi:10.1016/j.physletb.2015.03.040, arXiv:1502.02502.

[13] R. Andrade et al., "On the necessity to include event-by-event fluctuations in experimental evaluation of elliptical flow", *Phys. Rev. Lett.* **97** (2006) 202302, doi:10.1103/PhysRevLett.97.202302, arXiv:nucl-th/0608067.

[14] J. Qian, U. W. Heinz, and J. Liu, "Mode-coupling effects in anisotropic flow in heavy-ion collisions", *Phys. Rev. C* **93** (2016), no. 6, 064901, doi:10.1103/PhysRevC.93.064901, arXiv:1602.02813.

[15] D. Teaney and L. Yan, "Non linearities in the harmonic spectrum of heavy ion collisions with ideal and viscous hydrodynamics", *Phys. Rev. C* **86** (2012) 044908, doi:10.1103/PhysRevC.86.044908, arXiv:1206.1905.

[16] STAR Collaboration, "Azimuthal anisotropy at RHIC: The First and fourth harmonics", *Phys. Rev. Lett.* **92** (2004) 062301, doi:10.1103/PhysRevLett.92.062301, arXiv:nucl-ex/0310029.

[17] CMS Collaboration, "Measurement of higher-order harmonic azimuthal anisotropy in PbPb collisions at $\sqrt{s_{NN}}$ = 2.76 TeV", *Phys. Rev. C* **89** (2014), no. 4, 044906, doi:10.1103/PhysRevC.89.044906, arXiv:1310.8651.

[18] M. Luzum and J.-Y. Ollitrault, "Eliminating experimental bias in anisotropic-flow measurements of high-energy nuclear collisions", *Phys. Rev. C* **87** (2013), no. 4, 044907, doi:10.1103/PhysRevC.87.044907, arXiv:1209.2323.

[19] CMS Collaboration, "Centrality dependence of dihadron correlations and azimuthal anisotropy harmonics in PbPb collisions at $\sqrt{s_{NN}}$= 2.76 TeV", *Eur. Phys. J. C* **72** (2012) 10052, doi:10.1140/epjc/s10052-012-2012-3, arXiv:1201.3158.

[20] CMS Collaboration, "Observation of Long-Range Near-Side Angular Correlations in Proton-Proton Collisions at the LHC", *JHEP* **09** (2010) 091, doi:10.1007/JHEP09(2010)091, arXiv:1009.4122.

[21] CMS Collaboration, "Long-range and short-range dihadron angular correlations in central PbPb collisions at a nucleon-nucleon center of mass energy of 2.76 TeV", *JHEP* **07** (2011) 076, doi:10.1007/JHEP07(2011)076, arXiv:1105.2438.

[22] CMS Collaboration, "Observation of long-range near-side angular correlations in proton-lead collisions at the LHC", *Phys. Lett. B* **718** (2013) 795, doi:10.1016/j.physletb.2012.11.025, arXiv:1210.5482.

[23] CMS Collaboration, "The CMS Experiment at the CERN LHC", *JINST* **03** (2008) S08004, doi:10.1088/1748-0221/3/08/S08004.

[24] GEANT4 Collaboration, "GEANT4: A Simulation toolkit", *Nucl. Instrum. Meth. A* **506** (2003) 250–303, doi:10.1016/S0168-9002(03)01368-8.

[25] CMS Collaboration, "Description and performance of track and primary-vertex reconstruction with the CMS tracker", *JINST* **9** (2014), no. 10, P10009, doi:10.1088/1748-0221/9/10/P10009, arXiv:1405.6569.

[26] I. P. Lokhtin and A. M. Snigirev, "A Model of jet quenching in ultrarelativistic heavy ion collisions and high-p(T) hadron spectra at RHIC", *Eur. Phys. J. C* **45** (2006) 211–217, doi:10.1140/epjc/s2005-02426-3, arXiv:hep-ph/0506189.

[27] CMS Collaboration, "Multiplicity and transverse momentum dependence of two- and four-particle correlations in pPb and PbPb collisions", *Phys. Lett. B* **724** (2013) 213–240, doi:10.1016/j.physletb.2013.06.028, arXiv:1305.0609.